storage. ^{13}CO (99% ^{13}C) was purchased from Isotec. All reactions were conducted under argon with Schlenk techniques.[59] THF and 2-MeTHF were distilled from sodium/benzophenone ketyl and stored under argon in Schlenk vessels. CH_2Cl_2, HMPA, benzene-d_6, and toluene-d_8 were distilled from CaH_2 and stored under argon in Schlenk vessels. $Cr(acac)_3$ was used as a shiftless relaxation agent (~0.0001 M) in the ^{13}C NMR studies.[60]

Low-temperature IR spectra were recorded as previously described.[61] ^{13}C and ^{31}P NMR spectra were recorded at 75 and 121 MHz, respectively, on a Varian 300-VXR spectrometer.

Preparation of ^{13}CO-Enriched $FeCo_2(CO)_9(\mu_3$-PPh). A 0.50-g (0.94-mmol) amount of $FeCo_2(CO)_9(\mu_3$-PPh) in ~75 mL of benzene in a 500-mL Schlenk storage vessel was charged with ~1.0 atm of ^{13}CO. The solution was stirred at room temperature for 12 h and then at 50 °C for 3.0 h. IR analysis revealed negligible ^{13}CO incorporation in **1**. The flask was recharged with fresh ^{13}CO and irradiated for 6.0 h by using a medium-pressure Hg lamp. After the solution was cooled and vented, IR analysis indicated ~15-25% ^{13}CO enrichment had occurred. ^{13}CO-enriched **1** was purified by column chromatography under argon using Florisil and benzene as the eluant. Integration of the ^{13}C NMR resonance of the different carbonyl groups revealed that statistical ^{13}CO enrichment had occurred. Yield: 0.42 g (~84%). ^{13}C NMR (-80 °C; toluene-d_8): δ 218.7 (1 C, axial FeCO), 211.6 (2 C, equatorial FeCO), 201.0 (6 C, $Co(CO)_3$). ^{31}P NMR [-80 °C; THF/benzene-d_6 (5:1, v/v)]: δ 429.3.

Reaction of $FeCo_2(CO)_9(\mu_3$-PPh) with Reducing Agents. Since all the reduction reactions were conducted under similar conditions, only reaction between $FeCo_2(CO)_9(\mu_3$-PPh) and $[Et_3BH][Li]$ will be described in detail. To 20 mg (0.037 mmol) of $FeCo_2(CO)_9(\mu_3$-PPh) in 25 mL of THF at -78 °C was added 0.037 mL (0.037 mmol) of 1.0 M $[Et_3BH][Li]$ solution. The reaction was instantaneous as judged by the immediate discharge of the red solution and low-temperature analysis, which revealed only the presence of $\mathbf{2}^-$. ^{31}P NMR [-78 °C; 2-MeTHF/benzene-d_6 (4:1, v/v)]: δ 143.2. ^{13}C NMR [-90 °C; 2-MeTHF/benzene-d_6 (4:1, v/v)]: δ 222.9 (1 C, J_{P-C} = 18.5 Hz, axial FeCO), 221.8 (3 C, anionic $Co(CO)_3$), 215.8 (1 C, equatorial FeCO), 214.0 (1 C, equatorial FeCO), 208.6 (3 C, neutral $Co(CO)_3$).

Band-Shape Analysis. Since the acid and ester carbonyl stretching bands of $\mathbf{7}^-$ and $\mathbf{5}^-$ exhibit substantial overlap, the infrared band shapes of these CO bands were calculated by using a numerical procedure in order to determine the ratio of their areas. Absorbances were digitized from 1670 to 1560 cm^{-1} at 1-cm^{-1} intervals and entered into files of the university VAX 11/85 computer. Following baseline correction, the spectra were fit by a model consisting of Lorentzian band shapes, each characterized by a peak frequency (ν), maximum intensity (I), and half-width (fwhh) (Δ). Since the instrument resolution (2 cm^{-1}) is far less than the observed bandwidths (~20 cm^{-1}), it was unnecessary to convolute the model spectrum with a resolution (slit) function. The parameters were varied to minimize the squared deviation between the experimental and calculated intensities by using a nonlinear regression procedure.[62] Given that the area of a Lorentzian peak is proportional to the product of the bandwidth and the maximum intensity, the area ratio of the different anionic clusters is calculated easily as $A_2/A_1 = (I_2\Delta_2)/(I_1\Delta_1)$. The same procedure was also used in the area calculation of $\mathbf{3}^-$ and **3**[Li].

Acknowledgment. We thank George DeLong for NMR assistance. Financial support from the Robert A. Welch Foundation (Grant B-1039) and the UNT faculty research program is gratefully acknowledged.

(59) Shriver, D. F. *The Manipulation of Air-Sensitive Compounds*; McGraw-Hill: New York, 1969.
(60) Gansow, O. A.; Burke, A. R.; LaMar, G. N. *J. Chem. Soc., Chem. Commun.* **1972**, 456.
(61) Nunn, C. M.; Cowley, A. H.; Lee, S. W.; Richmond, M. G. *Inorg. Chem.* **1990**, *29*, 2105.
(62) Program STEPT: Chandler, J. P., Oklahoma State University. Quantum Chemistry Exchange Program, No. 307.

Contribution from the Department of Inorganic Chemistry and Department of Molecular Spectroscopy, University of Nijmegen, 6525 ED Nijmegen, The Netherlands

Low-Temperature ^{31}P NMR Studies of Metal Phosphine Clusters

R. P. F. Kanters,[†] P. P. J. Schlebos,[†] J. Bour,[†] J. J. Steggerda,*[,†] W. E. J. R. Maas,[‡] and R. Janssen[‡]

Received September 10, 1990

$[Au(PPh_3)(AuPPh_3)_7]^{2+}$, $[Pt(H)(PPh_3)(AuPPh_3)_7]^{2+}$, and $[Pt(Ag)(AuPPh_3)_8]^{3+}$ show sharp ^{31}P NMR resonances in solutions at room temperature although from the solid-state structure different phosphine sites are expected. This is due to fluxionality, the chemical exchange of different phosphorus sites. This process can be slowed by lowering the temperature, and in this slow-exchange regime the different phosphine sites can be assigned by means of ^{31}P homonuclear shift correlated spectroscopy methods. The tensor surface harmonics model, which is used for the description of the bonding in this type of clusters, offers a rationale for the trends in the observed magnitude of the coupling constants. Deviation of this model is observed for the toroidal clusters, in which the peripheral interactions are shown to be stronger than in the spheroidal clusters.

1. Introduction

Metal cluster compounds have attracted considerable interest for several years. They are considered to be compounds that can aid in understanding the behavior of small metal particles in solution. They are therefore important chemically in view of understanding catalytic behavior in which the ligands mimic the adsorbed species on a metal surface. From a physical point of view, they are important in investigating the breakdown of the macroscopic description of certain properties of metals, like conductivity, and electronic band structure as opposed to discrete molecular orbitals.

Bonding in metal phosphine clusters has been described in the past with a "porcupine" model.[1] This model stresses the importance of radial bonding in the cluster. The peripheral interactions are thought to be less important, which has been confirmed by Mingos et al. with the use of extended Hückel molecular orbital (EHMO) calculations.[2] For the total stabilization, the smaller peripheral interactions do contribute, since there are so many of them. The radial bonding model was confirmed by Mössbauer studies on homonuclear gold clusters showing that the data found for peripheral Au atoms are in the range that is found for linear mononuclear gold compounds.[3] Several years ago, Stone proposed the tensor surface harmonics theory (TSH), which provides us with a framework in which to describe molecular orbitals in terms of linear combinations of fragment orbitals of the peripheral metal-ligand groups.[4-6] Mingos et al. showed that the application of this theory to gold clusters is straightforward and enables us to predict the gross geometry in terms of prolate, oblate, and

* To whom correspondence should be addressed.
[†] Department of Inorganic Chemistry.
[‡] Department of Molecular Spectroscopy.

(1) King, R. B. *Prog. Inorg. Chem.* **1972**, *15*, 287.
(2) Mingos, D. M. P. *J. Chem. Soc., Dalton Trans.* **1972**, 133.
(3) Vollenbroek, F. A. Synthesis and Investigation of Gold Cluster Compounds. Ph.D. Thesis, University of Nijmegen, The Netherlands, 1979.
(4) Stone, A. J. *Mol. Phys.* **1980**, *41*, 1339.
(5) Stone, A. J. *Inorg. Chem.* **1981**, *20*, 563.
(6) Stone, A. J. *Polyhedron* **1984**, *3*, 1299.

0020-1669/91/1330-1709$02.50/0

spheroidal arrangements and the charge of the cluster compounds.[7-10] Until now, the only way to probe the bonding model with experiments is by electron count in combination with the geometry and ^{197}Au Mössbauer data.

^{31}P NMR spectrosopy would be a possible technique for investigating the bonding model. However, from ^{31}P proton-decoupled solution NMR spectra recorded at room temperature, it is found that they are not in agreement with what can be expected on the basis of the solid-state structure of the compounds. As a result of fast-exchange processes averaging the different phosphorus sites, only one chemical shift is found. Chemical-exchange studies have shown that intermolecular exchange of gold–phosphine or phosphine groups is too slow.[11] Also, not all clusters for which fluxionality is observed show intermolecular exchange of phosphines or gold phosphines. Intramolecular-exchange processes are more likely to be the cause of the fast exchange. This has very nicely been shown by Mingos et al., who prepared two geometrical modifications of the $[Au(AuP(p\text{-}C_6H_4Me)_3)_8]^{3+}$ cluster that interconvert rapidly in solution.[12] They also showed that the total energy difference between the two isomers is very small.

Investigations of fluxional behavior of gold phosphine clusters have been reported by van der Velden with the use of ^{31}P NMR variable-temperature measurements.[13] These investigations do not give us an answer as to whether the intramolecular process involves the migration of phosphines or gold phosphines in the cluster. This is due to the fact that with these experiments it is not possible to label both the Au and the P atom. Line shape analysis cannot give detailed information on the amount of energy involved in the rearrangement process because of unresolved couplings. The process by which the rearrangement occurs and the spin system are in our case too complex, e.g. a coupled eight-spin system in $[Au(PPh_3)(AuPPh_3)_7]^{2+}$. It is however possible to stop the fluxional behavior and observe the different intrinsic chemical shifts by lowering the temperature. This provides us with the possibility of investigating the coupling network of the cluster and comparing the results with what can be expected on the basis of the radial bonding model.

In this paper, we report the low-temperature ^{31}P NMR studies of two isostructural and isoelectronic $(S^\sigma)^2(P^\sigma)^6$ clusters, namely $[Pt(H)(PPh_3)(AuPPh_3)_7]^{2+}$ and $[Au(PPh_3)(AuPPh_3)_7]^{2+}$, for which the results will be compared to those of the $(S^\sigma)^2(P^\sigma)^4$ $[Pt(Ag)(AuPPh_3)_8]^{3+}$ cluster. We also present the assignment of ^{31}P resonances in these clusters in the slow-exchange regime, on the basis of homonuclear two-dimensional shift correlational spectroscopy (COSY). The COSY technique has proven to be a powerful tool for the elucidation of coupling networks.[14] Although it is most frequently used in ^{1}H NMR studies on large biomolecules, the same experiment can be successfully applied to other nuclei with homonuclear spin couplings.[15,16] 2D correlation methods not only help us in the assignment of ^{31}P resonances but also provide proof for the nonexistence of isomers at this temperature. In addition, we performed a solid-state ^{31}P COSY experiment in order to compare the geometry of the $[Pt(H)(PPh_3)(AuPPh_3)_7]^{2+}$ cluster in solution in the slow-exchange regime with its solid-state structure.

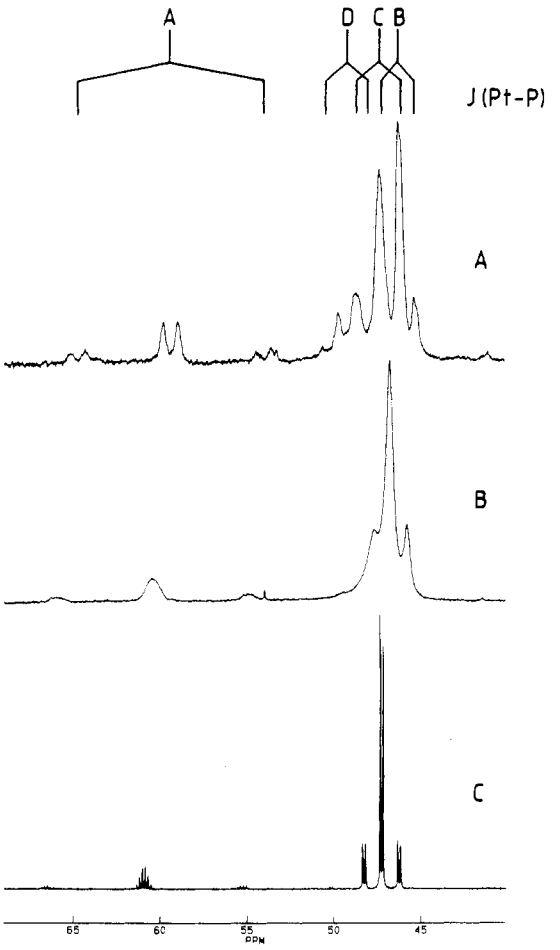

Figure 1. ^{31}P NMR spectra of $[Pt(H)(PPh_3)(AuPPh_3)_7]^{2+}$ at different temperatures: (A) 173 K; (B) 213 K; (C) 273 K.

2. Experimental Section

$[Pt(H)(PPh_3)(AuPPh_3)_7](NO_3)_2$,[17] $[Au(PPh_3)(AuPPh_3)_7](NO_3)_2$,[18] and $[Pt(AgNO_3)(AuPPh_3)_8](NO_3)_2$[19] were prepared according to the literature.

^{31}P proton-decoupled NMR experiments in solution were performed on a Bruker AM-500 spectrometer operating at 202.46 MHz for ^{31}P. The compounds were dissolved in CD_2Cl_2 in the temperature range 200–300 K and in a 1:1 mixture of $CD_2Cl_2/CHClF_2$ below 200 K. Trimethyl phosphate (TMP) was added as an internal reference (0 ppm).

Phase-sensitive proton-decoupled ^{31}P COSY spectra were recorded with double-quantum filtering.[20] After zero-filling to 1024 times 1024 data points and multiplication by a squared-sine filter, the free induction decays were Fourier transformed to yield a two-dimensional spectrum. Subsequently the 2D spectra were symmetrized. A relaxation delay of 2.5 s was used, and before addition of the FID's, eight dummy scans were applied to ensure steady-state magnetization. The spectrum of $[Pt(H)(PPh_3)(AuPPh_3)_7]^{2+}$ was recorded at 173 K in a $CD_2Cl_2/CHClF_2$ mixture. A total of 128 FID's were recorded with a sweep width of 6100 Hz, each FID containing 128 data points. The spectrum of $[Au(PPh_3)(AuPPh_3)_7]^{2+}$ was recorded at 203 K in a CD_2Cl_2 solution. A total of 256 FID's were recorded, with a sweep width of 7100 Hz and a time domain of 256 points. The spectrum of $[Pt(Ag)(AuPPh_3)_8]^{3+}$ was recorded at 233 K in a CD_2Cl_2 solution with a time domain of 200 points and a sweep width of 6100 Hz. A total of 200 t1-FID's were acquired.

The ^{31}P solid-state experiments were performed on a Bruker CXP-300 spectrometer, operating at 300.1 MHz for protons and 121.4 MHz for phosphorus. ^{31}P spectra were recorded by using cross-polarization and

(7) Mingos, D. M. P.; Hall, K. P. *Prog. Inorg. Chem.* **1982**, *32*, 239.
(8) Mingos, D. M. P.; Hall, K. P.; Gilmour, D. I. *J. Organomet. Chem.* **1984**, *268*, 275.
(9) Mingos, D. M. P. *Polyhedron* **1984**, *3*, 1289.
(10) Mingos, D. M. P. *Proc. R. Soc. London, A* **1982**, *308*, 25.
(11) Vollenbroek, F. A.; van den Berg, J. P.; van der Velden, J. W. A.; Bour, J. J. *Inorg. Chem.* **1980**, *19*, 2685.
(12) Briant, C. E.; Hall, K. P.; Mingos, D. M. P. *J. Chem. Soc., Chem. Commun.* **1984**, 290.
(13) van der Velden, J. W. A. Preparation and Properties of Gold Cluster Compounds. Ph.D. Thesis, University of Nijmegen, The Netherlands, 1983.
(14) Ernst, R. R.; Bodenhausen, G.; Wokaun, A. *Principles of Nuclear Magnetic Resonance in One and Two Dimensions*; The International Series of Monographs on Chemistry 14; Clarendon Press: Oxford, U.K., 1987.
(15) Brevard, C.; Schimpf, R.; Tourne, G.; Tourne, C. M. *J. Am. Chem. Soc.* **1983**, *105*, 7059.
(16) Venable, T. L.; Hutton, W. C.; Grimes, R. N. *J. Am. Chem. Soc.* **1984**, *106*, 29.
(17) Kanters, R. P. F.; Bour, J. J.; Schlebos, P. P. J.; Bosman, W. P.; Behm, H.; Steggerda, J. J.; Pignolet, L. H. *Inorg. Chem.* **1989**, *28*, 2591.
(18) Steggerda, J. J.; Bour, J. J.; van der Velden, J. W. A. *Recl. Trav. Chim. Pays-Bas* **1982**, *101*, 164.
(19) Kanters, R. P. F.; Schlebos, P. P. J.; Bour, J. J.; Bosman, W. P.; Smits, J. M. M.; Beurskens, P. T.; Steggerda, J. J. *Inorg. Chem.* **1990**, *29*, 324.
(20) Piantini, U.; Sørenson, O. W.; Ernst, R. R. *J. Am. Chem. Soc.* **1982**, *104*, 6800.

Table I. ^{31}P NMR Data (δ, ppm; J, Hz)

site	int	δ	J(P–P)	^2J(Pt–P)	J(Ag–P)
		$[Pt(H)(PPh_3)(AuPPh_3)_7]^{2+}$ (173 K)			
A1	1	59.4	145 (AD)	2168	
D2	1	49.3		389	
C3	3	47.3	85 (AC)	480	
B4	3	46.0	85 (BC)	358	
		$[Au(PPh_3)(AuPPh_3)_7]^{2+}$ (203 K)			
A1	1	68.7	62 (AC)		
C2	3	51.9	87 (BC)		
B3	3	49.1			
D4	1	47.0	195 (AD)		
		$[Pt(Ag)(AuPPh_3)_8]^{3+}$ (233 K)			
B1	2	64.0	70 (BC)	536	
A2	1	61.2	70 (AE)	452	50
C3	2	55.3	70 (CD)	320	
E4	1	50.4	70 (BE)	400	100
D5	2	48.8	70 (BD)	500	

magic angle spinning techniques. A phase-sensitive experiment was performed by using a spinning frequency of 5 kHz. Radio frequency strengths were 50 kHz for both frequencies. A total of 256 FID's were acquired with a sweep width of 20 kHz and a time domain of 256 data points. Prior to Fourier transformation, the data were zero-filled to 2048 times 2048 data points and multiplied by a squared-sine filter.

3. Results

3.1. $[Pt(H)(PPh_3)(AuPPh_3)_7]^{2+}$. $^{31}P\{^1H\}$ NMR spectra at several temperatures are shown in Figure 1. In the fast-exchange regime the spectrum consists of two sites: Pt–P δ = 60.9 ppm, with ^3J(P–P)(octet) = 33.7 Hz and ^1J(P–Pt)(doublet) = 2290 Hz; Au–P δ = 47.2 ppm, with ^3J(doublet) = 33.7 Hz and ^2J(P–Pt)(doublet) = 409.9 Hz. Lowering the temperature results in a broadening of the lines, and the slow-exchange regime is reached at about 185 K. The spectrum recorded at 173 K (Figure 1A) can be interpreted as four phosphorus sites with platinum satellites. Two sites have an intensity of 1, and the other two, an intensity of 3. Due to the broad lines, no reliable couplings can be obtained from these spectra.

To obtain better values for couplings and shifts and to investigate the coupling network, a proton-decoupled phase-sensitive COSY experiment was performed at 173 K in $CD_2Cl_2/CHFCl_2$. The symmetrized spectrum is shown in Figure 2A, and the obtained shifts and couplings are given in Table I. The solid-state COSY spectrum is shown in Figure 2B.

3.2. $[Au(PPh_3)(AuPPh_3)_7]^{2+}$. The slow-exchange regime is reached at 215 K. The spectrum recorded at 203 K is shown in Figure 3. In this spectrum we can see four phosphorus sites, of which two have an intensity of 1 and the other two an intensity of 3.

To investigate the coupling network in this cluster, a proton-decoupled double-quantum-filtered phase-sensitive COSY experiment was performed at 203 K in a CD_2Cl_2 solution. The symmetrized spectrum is shown in Figure 4, and the obtained data are given in Table I.

3.3. $[Pt(Ag)(AuPPh_3)_8]^{3+}$. The slow-exchange regime is reached at about 250 K. Below this temperature, we can distinguish five phosphorus shifts with their satellites. Two of the sites have intensity 1 and the other three intensity 2. The spectrum at 233 K is shown in Figure 5. The peaks are too broad to show the ^{31}P and ^{107,109}Ag couplings.

The symmetrized proton-decoupled homonuclear shift correlated phase-sensitive spectrum with double-quantum filtering at 233 K is shown in Figure 6. The obtained values for the chemical shifts and couplings are given in Table I.

4. Interpretation of the Spectra

4.1. $[Au(PPh_3)(AuPPh_3)_7]^{2+}$ and $[Pt(H)(PPh_3)(AuPPh_3)_7]^{2+}$. The solid-state X-ray structures of these compounds have been elucidated.[17,21] They both show a central metal atom surrounded

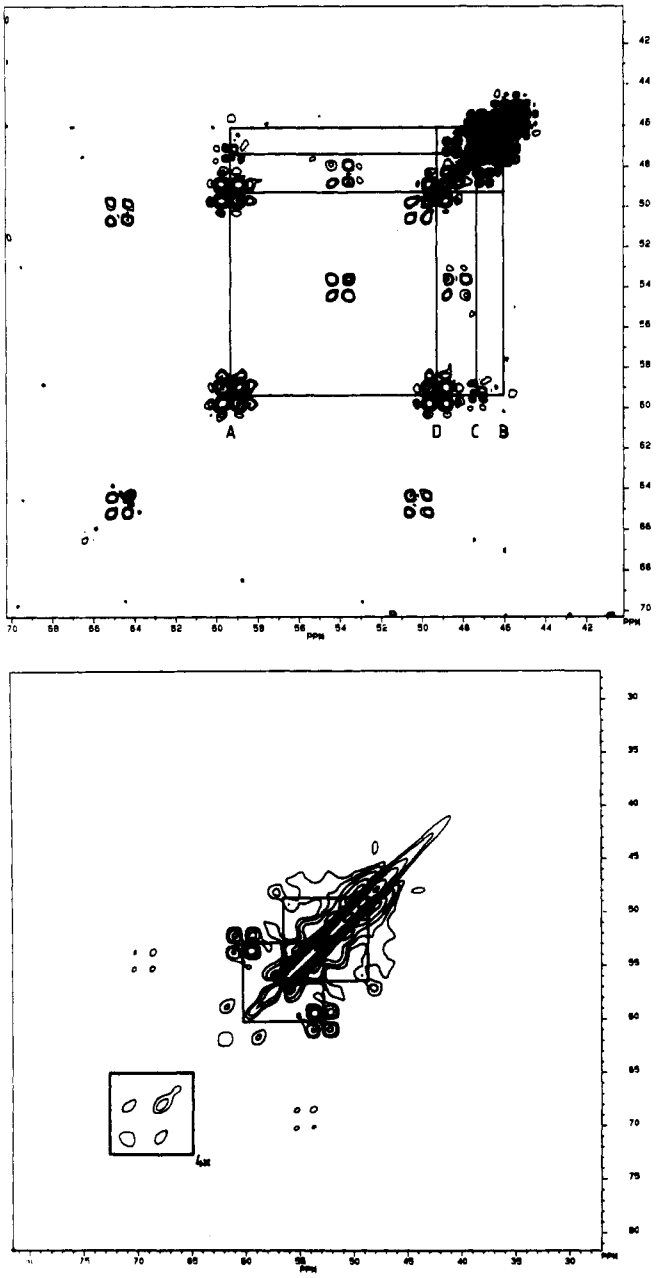

Figure 2. Symmetrized phase-sensitive COSY spectra in solution (A, top) at 173 K and the solid state (B, bottom) at room temperature of $[Pt(H)(PPh_3)(AuPPh_3)_7]^{2+}$. The intensity in the insert in part B is magnified by 4.

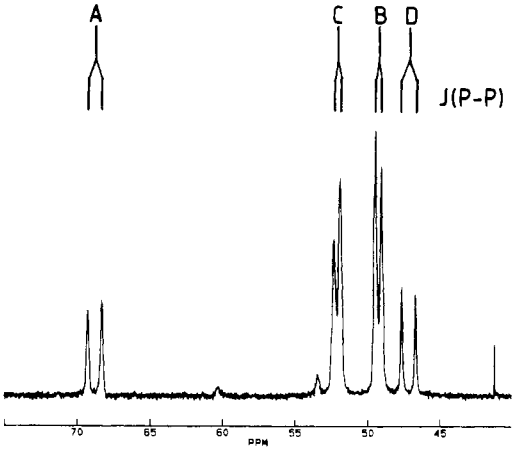

Figure 3. Slow-exchange ^{31}P NMR spectrum of $[Au(PPh_3)(AuPPh_3)_7]^{2+}$ at 203 K.

(21) Manassero, M.; Naldini, L.; Sansoni, M. *J. Chem. Soc., Chem. Commun.* **1979**, 285.

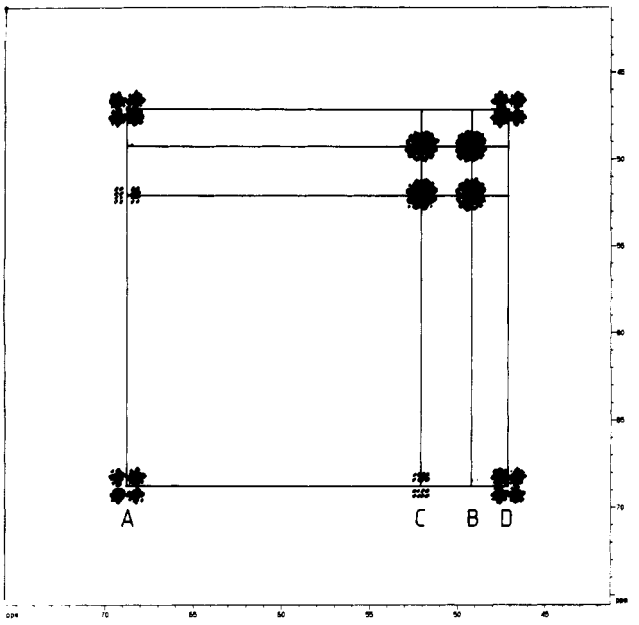

Figure 4. Symmetrized phase-sensitive COSY spectrum of $[Au(PPh_3)(AuPPh_3)_7]^{2+}$ at 203 K.

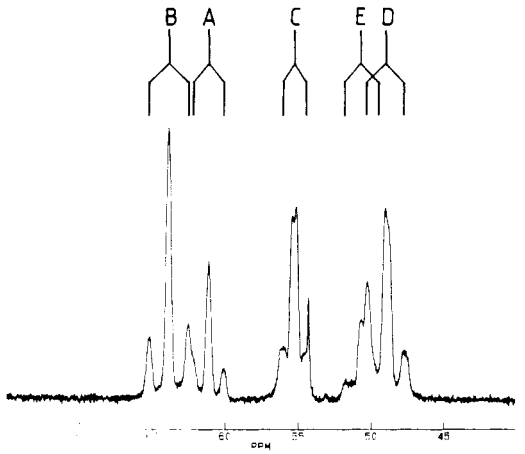

Figure 5. Slow-exchange ^{31}P NMR spectrum of $[Pt(Ag)(AuPPh_3)_8]^{3+}$ at 233 K.

by one PPh_3 and seven $AuPPh_3$ groups in a nearly cubic arrangement. The hydrogen position in $[Pt(H)(PPh_3)(AuPPh_3)_7]^{2+}$ could not be determined. It is expected to be fluxional over the faces of the cube that are adjacent to the C_3 axis. The structure and labeling of the phosphorus sites are shown in Figure 7. The C_{3v} geometry gives rise to four phosphine sites with a ratio of A:B:C:D = 1:3:3:1. The similarity in splitting pattern and therefore the coupling network of the solid-state COSY spectrum of $[Pt(H)(PPh_3)(AuPPh_3)_7]^{2+}$ compared to the one at low temperature in solution suggests that the geometry of the cluster is the same in both cases. In both spectra we can clearly see the crosspeak between sites A and D. Sites B and C cannot be assigned in the solid-state spectrum, since the coupling of site C with A is too small to be detected. The relative ordering of the chemical shifts is different for the solid state compared to that found in solution, which can be caused by packing effects. The solid-state spectrum shows that, due to the phase-sensitive detection in combination with the large line widths compared to the active coupling constant, cancelation of the resulting antiphase peaks occurs. This results in low intense crosspeaks, or even diagonal peaks, and maxima of the peaks suggesting a larger coupling than the actual value. This is most clearly seen for site A, for which the diagonal peak suggests a larger coupling than the crosspeak with site D because the line width of the diagonal peaks is larger, since no double-quantum-filtering has been done. Therefore the actual coupling constants are not very accurate when the coupling

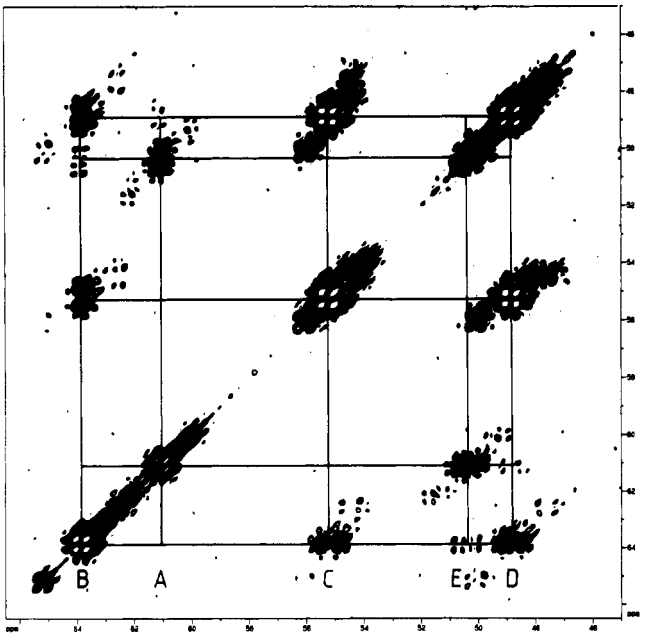

Figure 6. Symmetrized phase-sensitive COSY spectrum of $[Pt(Ag)(AuPPh_3)_8]^{3+}$ at 233 K.

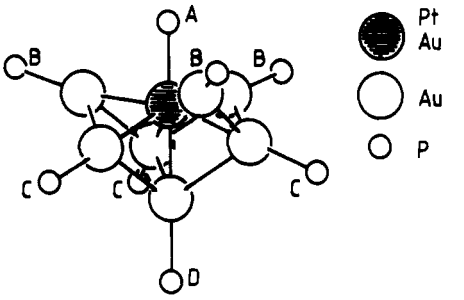

Figure 7. Idealized structures of $[Au(PPh_3)(AuPPh_3)_7]^{2+}$ and $[Pt(H)(PPh_3)(AuPPh_3)_7]^{2+}$ showing the four phosphorus sites and labeling.

constant is smaller than or equal to the line width of the resonances.

The isostructurality of these compounds can be rationalized by the same coordination number—not taking into account the hydrogen—of the central metal atom and the isoelectronicity of the compounds. They are both $(S^{\sigma})^2(P^{\sigma})^6$ compounds, and according to the TSH bonding model, they should have spherically arranged skeletons. The strongly radial nature of the bonding in the σ clusters suggests that the spin–spin coupling is mediated through the central metal atom. As a consequence, the angles of the peripheral groups with the central atom (L–M–L; L is a peripheral group and M is the central metal atom) will strongly influence the magnitude of the coupling. The coupling is maximal for an angle of 180°.

From inspection of the line intensities and the magnitude of the ^3J couplings compared to the other ^4J couplings, it is clear that peaks 1 and 2 for $[Au(PPh_3)(AuPPh_3)_7]^{2+}$ (Figure 4) and 1 and 4 for $[Pt(H)(PPh_3)(AuPPh_3)_7]^{2+}$ (Figure 2) correspond to A and D. The variable-temperature series of $[Pt(H)(PPh_3)(AuPPh_3)_7]^{2+}$ and the magnitude of the platinum–phosphorus coupling show that peak 1 corresponds to the phosphine bonded to the central metal atom.

The other ^3J couplings that should occur in these clusters are those between A and B and between A and C. Because of the forementioned dependence of the value of the coupling constant on the angle L–M–L, site C is assigned to peak 2 for $[Au(PPh_3)(AuPPh_3)_7]^{2+}$ and to peak 3 for $[Pt(H)(PPh_3)(AuPPh_3)_7]^{2+}$. This leaves peaks 3 and 4 assigned to B for $[Au(PPh_3)(AuPPh_3)_7]^{2+}$ and $[Pt(H)(PPh_3)(AuPPh_3)_7]^{2+}$, respectively. In Figure 4, we can more clearly see the pattern of the crosspeak between sites A and C. Superposed upon the small active coupling

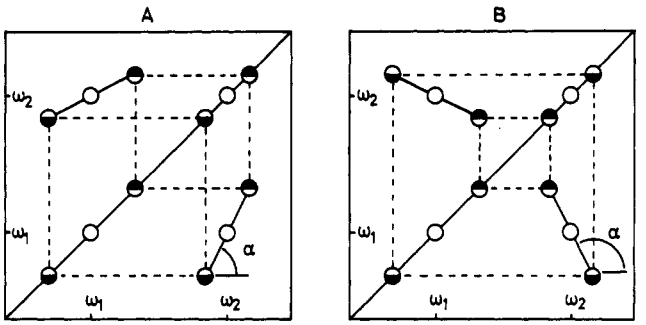

Figure 8. Construction of satellites of crosspeaks showing the difference between coupling of equal (A) and opposite (B) signs.

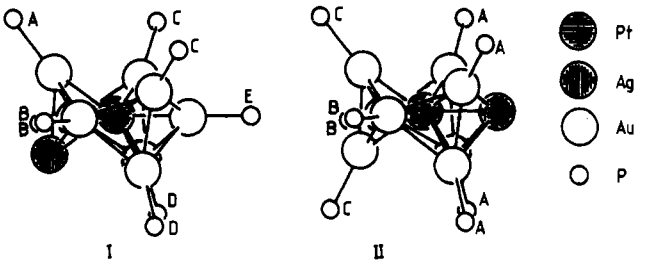

Figure 9. Two possible isomers of $[Pt(Ag)(AuPPh_3)_8]^{3+}$ showing the five sites for isomer I and the three sites for isomer II.

J(A–C) (which results in quartets for A, of which only the central two lines are visible) and a doublet for C, we observe the passive A–D and B–C couplings. From the very low intense signal found for the crosspeak AB, we can see that this coupling is smaller than that of CD, since cancellation is more complete.

The relative signs of the Pt–P couplings can also be determined from these spectra.[14] The isotopomer with ^{195}Pt gives rise to diagonal satellites as well as the crosspeak satellites. The resulting pattern for the crosspeaks is that of a heteronuclear passive coupling. In the crosspeak we can see whether, for instance, spin-up for platinum is stabilized in both sites, giving rise to a pattern as shown in Figure 8A, and therefore coupling constants of equal signs. The other possibility is that of different signs for the coupling, resulting in a pattern as shown in Figure 8B. So, if the sign of tan α (see Figure 8) is positive, then both couplings have the same sign: tan $\alpha = J_{1,X}/J_{2,X}$. In our case, the ^1J and ^2J platinum–phosphorus couplings are of the same sign for all shifts.

The existence of the ^2J platinum couplings in $[Pt(H)(PPh_3)(AuPPh_3)_7]^{2+}$ enables us to compare the measured coupling constants with the radial bond strengths. To do this, we performed an extended Hückel molecular orbital calculation on the idealized $[Pt(P)(AuP)_7]^+$ cluster with the platinum atom in a cubic environment and no H^+. The trends observed in the radial metal–metal overlap populations, 0.32, 0.31, and 0.29, agree with the measured trend in couplings constants: 480, 389, and 358 Hz for sites C, D, and B, respectively.

4.2. $[Pt(Ag)(AuPPh_3)_8]^{3+}$. The solid-state structure of $[Pt(Ag)(AuPPh_3)_8]^{3+}$ can be considered as three staggered triangles with silver in the top, or bottom, triangle and platinum in the center of the middle one.[19] This geometry leads to the possibility of two isomers in solution, as shown in Figure 9. Inspection of this figure shows that for isomer I we can expect five different phosphorus sites with a ratio of A:B:C:D:E = 1:2:2:2:1 and for isomer II three sites with a ratio of A:B:C = 2:2:4. The slow-exchange spectrum shows five different phosphine sites, in agreement with the expected number for isomer I, which also is the isomer found in the solid state as determined by X-ray diffraction.[19] Extended Hückel molecular orbital calculations show that the total energy of isomer I is −1793.3 eV, which is lower than the −1792.9 eV for isomer II. Also, the HOMO–LUMO gap for I is larger than that for II (2.0 and 1.5 eV, respectively), which agrees with the general finding that the most electronegative atom, in this case Au, will stabilize the molecule if it is at a position with the highest connectivity. This also suggests that the most stable isomer will be I.

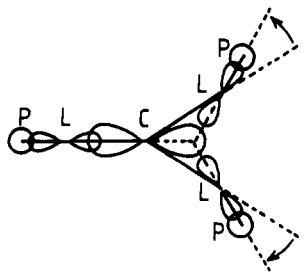

Figure 10. Intersection through the plane perpendicular to the torus plane in $[Pt(Ag)(AuPPh_3)_8]^{3+}$ showing the effect of the decrease in radial bond angle on the overlap. C = central metal atom (M, as defined in text).

The assignment of sites A and E is straightforward because the bonding model suggests J(E–Ag) to be larger than J(A–Ag). Therefore peak 2 is assigned to site A and peak 4 to E. The occurrence of a crosspeak between peaks 1 and 4 in the COSY spectrum (Figure 6) suggests that peak 1 may be assigned to site B. The existence of a low intense crosspeak between site A and peak 5 suggests that the latter is site D, on the basis of the angular dependence of the radial coupling. The remaining peak 3 is therefore site C.

5. Discussion

The coupling in $[Au(PPh_3)(AuPPh_3)_7]^{2+}$ and $[Pt(H)(PPh_3)(AuPPh_3)_7]^{2+}$ mainly takes place through the radial σ bonds, which is in agreement with the bonding model for this kind of metal phosphine cluster. Both clusters have an $(S^\sigma)^2(P^\sigma)^6$ electron configuration, suggesting that in the ideal case the radial overlaps are evenly distributed among the spherically arranged ligands. The $[Pt(Ag)(AuPPh_3)_8]^{3+}$ cluster with the $(S^\sigma)^2(P^\sigma)^4$ configuration has the largest electron density in the torus plane. This electron density is caused by the occupancy of the $P^\sigma_{x,y}$ molecular orbitals. The resulting electron distribution resembles the shape of a torus with platinum in the center. The peripheral metal sp hybrids will therefore overlap more strongly with these orbitals when the Au–P bond vector is pointed toward the center of the ring and not the center of the torus; see Figure 10. This bending away from the torus plane of the phosphine outside the plane is also found in the solid state. Another reason may be the large steric hindrance of the phosphines by the already crowded torus plane.

The result is an increase of the angle between the atoms on the same side of the platinum atom and an increment in their coupling. Also, the Au–Pt–Au angle between the gold atom in the torus and that out of the torus is decreased, and accordingly the phosphorus–phosphorus coupling constant diminishes. This effect is a low-symmetry perturbation on the initial spherical model, and the fact that it is measurable in solution suggests that this decrease in radial bond angles as found in the solid state is not a packing effect.

The determination of the kinetics and the activation parameters for the intramolecular exchange processes in these cluster compounds from the NMR data is complicated because of the many sites present. Further, the possibility that the fluxionality is not due to a single concerted process should be considered. The results of such a study are, however, of great interest, as any conclusion about the molecular mechanism of the exchange process should wait. We will return to these questions in later publications.

6. Conclusion

Lowering the temperature of solutions of the investigated metal phosphine clusters shows that it is possible to slow down and even stop the chemical exchange of the phosphine sites. The geometry of the structure in absence of fluxionality is similar to that found in the solid state, which when different isomers can be formed is the thermodynamically more stable one. By recording COSY spectra, we were able to assign the chemical shifts to the sites found in the solid-state structures. The interpretation of the spectra supports the radial bonding model specially for the $(S^\sigma)^2(P^\sigma)^6$

clusters and the expected angular dependence of the radial P-P coupling. For the toroidal $(S^{\sigma})^2(P^{\sigma})^4$ cluster $[Pt(Ag)(AuPPh_3)_8]^{3+}$, we observed that the coupling constants are dependent not only on the Au-Pt-Au angle but also on the Pt-Au-P angle, which for this type of clusters more strongly deviates from linearity when the Au-P group lies above or below the torus plane.

Acknowledgment. This work was supported by the Dutch Research Foundation (NWO/SON). We thank Mr. J. J. M. Joordens and Ms. G. H. Nachtegaal for technical assistance at the Dutch National NMR facility at Nijmegen. Prof. W. S. Veeman is thanked for helpful discussions and critically reading the manuscript.

Contribution from the Departments of Chemistry, Yale University, New Haven, Connecticut 06511, and Oklahoma State University, Stillwater, Oklahoma 74078-0447

Ruthenium in an O Donor Environment: Properties and Reactions of η^3-$(RPO(C_6H_4O)_2)^{2-}$, η^3-$(CpCo(PO(OEt)_2)_3)^-$ and η^3-$HC(POPh_2)_3$ Complexes of Ruthenium

Robin S. Tanke,*[1] Elizabeth M. Holt,[2] and Robert H. Crabtree[1]

Received April 16, 1990

The tridentate oxygen donor ligands η^3-$(RPO(C_6H_4O)_2)^{2-}$ (bipo), η^3-$(CpCo(PO(OEt)_2)_3)^-$ (L'), and η^3-$HC(POPh_2)_3$ (Htriso) are shown to form a number of organometallic Ru(II) complexes. A single crystal X-ray study of **2b**, $[(\eta^6\text{-ArH})Ru\{\eta^3\text{-}RPO(C_6H_4O)_2\}]$ (R = Ph, ArH = *p*-cymene) shows that the phosphorus-containing ligand is bound to the metal via the two phenolate groups and the phosphine oxide oxygen. The complex **2b** crystallizes in the space group $P\bar{1}$ with lattice constants a = 10.407 (6) Å, b = 14.334 (6) Å, c = 13.25 (1) Å, α = 75.85 (5)°, β = 129.85 (4)°, γ = 81.28 (4)°, V = 1340 (1) Å^3, Z = 2, R = 6.6%, and R_w = 11.4%. The arene and carbonyl complexes $[HtrisoRu(\eta^6\text{-ArH})](SbF_6)_2$, $[L'Ru(\eta^6\text{-ArH})](SbF_6)$, $[HtrisoRu(CO)_3](SbF_6)_2$, and $[L'Ru(CO)_3](SbF_6)$ were prepared. $[L'Ru(CO)_3](SbF_6)$ reacts with Me_3NO to give $[L'Ru(CO)(solvent)_2](SbF_6)$ (solvent = THF, dioxane) or $L'Ru(CO)_2(OR)$ (R = Me, Ac, $CH(Me)_2$; solvent = MeOH, AcOH, Me_2CHOH). These solvento and alkoxide complexes are exceptionally stable to dissociation and β-elimination, respectively.

Introduction

We still know very little about how an O donor ligand environment affects organometallic chemistry and homogeneous catalysis.[3] The demonstration[4] of heterogeneous catalysis by site-isolated organometallic fragments supported on oxide surfaces suggests that interesting results will be found. Kläui and coworkers[5] have shown that the ν(CO) values for $\{CpCo(R_2PO)_3\}M(CO)_n$ are similar to those for alumina-supported metal carbonyl fragments.[6] The studies of Feher et al.[7] with trisilicates and work with $P_3O_9^{3-}$ by Klemperer et al.[8] have demonstrated that tridentate O ligands can form stable organometallic complexes that show unusual chemical reactivity.

We are interested in O donor ligands not only to expand the study of heterogeneous catalysis but also to extend the field of organometallic chemistry beyond the P and C ligand set that currently dominates the field. We have shown[9] that Grim's[10] triso ligand stabilizes Ir(I), Ir(III), and Ir(V) complexes that are active homogeneous catalysts for a variety of hydrosilylation reactions. In this paper, we discuss our results for Ru with the tridentate oxygen donor ligands, η^3-$(RPO(C_6H_4O_2)^{2-}$ (bipo), η^3-$(CpCo(PO(OEt)_2)_3)^-$ (L') and η^3-$HC(POPh_2)_3$ (Htriso).

Table I. Crystal Data for $RuPO_3C_{28}H_2$ (**2b**)

formula: $RuPO_3C_{28}H_{27}$	μ(Mo Kα) = 6.555 cm^{-1}
MW = 543.56	λ(Mo Kα) = 0.71069 Å
a = 10.407 (6) Å	D_{calc} = 1.347 g cm^{-3}
b = 14.334 (6) Å	Z = 2
c = 13.25 (1) Å	space group: $P\bar{1}$ (No. 2)
α = 75.85 (5)°	no. of measd reflcns: 4758
β = 129.85 (4)°	no. of obs reflcns: 3492
γ = 81.28 (4)°	octants measd: $\pm h,+k,\pm l$
V = 1340 (1) Å^3	R = 6.6%
F(000) = 556	R_w = 11.4%

Results

The protonated ligands, $RP(O)(o\text{-}C_6H_4OH)_2$ (R = *o*-hydroxyphenyl (**1a**), phenyl (**1b**), *n*-propyl (**1c**)) react with 2 equiv

(1) Yale University.
(2) Oklahoma State University.
(3) (a) LaPointe, R. E.; Wolczanski, P. T.; Van Duyne, G. D. *Organometallics* **1985**, *4*, 1810. (b) Chisholm, M. H.; Hoffman, D. M.; Huffman, J. *Chem. Soc. Rev.* **1985**, *14*, 69. (c) Besecker, C. J.; Klemperer, W. G. *J. Am. Chem. Soc.* **1980**, *102*, 7598. (d) Day, V. W.; Besecker, C. J.; Klemperer, W. G. *J. Am. Chem. Soc.* **1982**, *104*, 6158. (e) Day, V. W.; Earley, C. W.; Klemperer, W. G.; Maltbie, D. *J. Am. Chem. Soc.* **1985**, *107*, 8261. (f) Besecker, C. J.; Day, V. W.; Klemperer, W. G.; Thompson, M. R. *J. Am. Chem. Soc.* **1984**, *106*, 4125. (g) Finke, R. G.; Droege, M. W. *J. Am. Chem. Soc.* **1984**, *106*, 7274. (h) Edlund, D. J.; Saxton, R. J.; Lyon, D. K.; Finke, R. G. *Organometallics* **1988**, *7*, 1692. (i) Zhang, N.; Mann, C. M.; Shapley, P. A. *J. Am. Chem. Soc.* **1988**, *110*, 6591. (j) Veitsch, P. M.; Allan, J. R.; Blake, A. J.; Schröder, M. *J. Chem. Soc., Dalton Trans.* **1987**, 2853. (k) Haiduc, I.; Silaghi-Dumitrescu, I. *Coord. Chem. Rev.* **1986**, *74*, 127. (l) Finke, R. G.; Lyon, D. K.; Nomiya, K.; Sur, S.; Mizzuno, N. *Inorg. Chem.* **1990**, *29*, 1784. (m) Lyon, D. K.; Finke, R. G. *Inorg. Chem.* **1990**, *29*, 1787. (n) Day, V. W.; Klemperer, W. G.; Main, D. J. *Inorg. Chem.* **1990**, *29*, 2345.
(4) (a) Yermakov, Yu. I.; Kuznetsov, B. N.; Zakharov, V. *Catalysis by Supported Complexes*; Elsevier: Amsterdam, 1981. (b) Ballard, D. G. H. *Adv. Catal.* **1973**, *23*, 263. (c) Schwartz, J. *Acc. Chem. Res.* **1985**, *18*, 302. (d) Gates, B. C.; Lamb, H. H. *J. Mol. Catal.* **1989**, *52*, 1.
(5) (a) Kläui, W.; Müller, A.; Eberspech, W.; Boese, R.; Goldberg, I. *J. Am. Chem. Soc.* **1987**, *109*, 164. (b) Kläui, W. Personal communication, 1989.
(6) (a) Duivenvoorden, F. B. M.; Koningsberger, D. C.; Uh, Y. S.; Gates, B. C. *J. Am. Chem. Soc.* **1986**, *108*, 6254. (b) van't Blik, H. F. J.; van Zon, J. B. A. D.; Huizinga, T.; Vis, J. C.; Koningsberger, D. C. *J. Am. Chem. Soc.* **1985**, *107*, 3139. (c) Kirlin, P. S.; DeThomas, F. A.; Bailey, J. W.; Gold, H. S.; Dybowski, C.; Gates, B. C. *J. Phys. Chem.* **1986**, *90*, 4882.
(7) Feher, F. J. *J. Am. Chem. Soc.* **1986**, *108*, 3851.
(8) (a) Besecker, C. J.; Day, V. W.; Klemperer, W. G. *Organometallics* **1985**, *4*, 564. (b) Besecker, C. J.; Klemperer, W. G. *J. Organomet. Chem.* **1981**, *205*, C31. (c) Day, V. W.; Klemperer, W. G.; Lockledge, S. P.; Main, D. J. *J. Am. Chem. Soc.* **1990**, *112*, 2031.
(9) (a) Tanke, R. S.; Crabtree, R. H. *J. Chem. Soc., Chem. Commun.* **1990**, 1056. (b) Tanke, R. S.; Crabtree, R. H. *J. Am. Chem. Soc.* **1990**, *112*, 7984. (c) Tanke, R. S.; Crabtree, R. H. *Organometallics* **1991**, *10*, 415.
(10) Grim, S. O.; Sangokoya, S. A.; Colquhoun, I. J.; McFarlane, W.; Khanna, R. K. *Inorg. Chem.* **1986**, *25*, 2699.

0020-1669/91/1330-1714$02.50/0